Mapping Glycosaminoglycan−Hydroxyapatite Colloidal Gels as Potential Tissue Defect Fillers

S. Connor Dennis,[†,‡] Michael S. Detamore,[†,‡] Sarah L. Kieweg,[†,§] and Cory J. Berkland*[,†,‡,‖]

[†]Bioengineering Program, [‡]Chemical and Petroleum Engineering Department, [§]Mechanical Engineering Department, and [‖]Pharmaceutical Chemistry Department, University of Kansas, Lawrence, Kansas 66045, United States

S *Supporting Information*

ABSTRACT: Malleable biomaterials such as Herschel−Bulkley (H−B) fluids possess shear responsive rheological properties and are capable of self-assembly and viscoelastic recovery following mechanical disruption (e.g., surgical placement via injection or spreading). This study demonstrated that the addition of moderate molecular weight glycosaminoglycans (GAGs) such as chondroitin sulfate (CS) (M_w = 15−30 kDa) and hyaluronic acid (HA) (M_w = 20−41 kDa) can be used to modify several rheological

properties including consistency index (K), flow-behavior index (n), and yield stress (τ_y) of submicrometer hydroxyapatite (HAP) ($D_{avg} \leq 200$ nm) colloidal gels. GAG−HAP colloidal mixtures exhibited substantial polymer−particle synergism, likely due to "bridging" flocculation, which led to a synergistic increase in consistency index ($K_{GAG-HAP} \geq K_{GAG} + K_{HAP}$) without compromising shear-thinning behavior ($n < 1$) of the gel. In addition, GAG−HAP colloids containing high concentrations of HAP (60−80% w/v) exhibited substantial yield stress ($\tau_y \geq 100$ Pa) and viscoelastic recovery properties ($G'_{recovery} \geq 64\%$). While rheological differences were observed between CS−HAP and HA−HAP colloidal gels, both CS and HA represent feasible options for future studies involving bone defect filling. Overall, this study identified mixture regions where rheological properties in CS−HAP and HA−HAP colloidal gels aligned with desired properties to facilitate surgical placement in non-load-bearing tissue-filling applications such as calvarial defects.
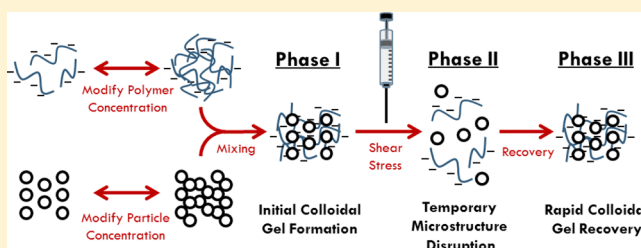
1. INTRODUCTION

Developing malleable biomaterials for filling tissue defects is desirable for minimally invasive surgical repair and potential regeneration of bone defects.[1−3] Minimally invasive surgery reduces the risk of infection and scar formation while also decreasing patient discomfort and cost of treatment.[1−3] Malleable biomaterials with shear responsive rheological properties, such as Herschel−Bulkley (H−B) fluids which possess favorable yield stress and shear-thinning behavior, may be injected or extruded to fill irregular-shaped bone defects. It may also be necessary for these materials to have sufficient viscoelastic recovery kinetics following placement to ensure retention at the defect site. An ideal H−B fluid biomaterial candidate would facilitate surgical placement and site retention with desirable shear responsive properties and viscoelastic properties, respectively.

Many injectable scaffolds exhibit thickening or stiffening after placement via *in situ* chemical cross-linking in the presence of water, heat, light, or other stimuli; however, concerns exist where unreacted reagents or catalysts may persist and impose localized cytotoxicity or adversely affect encapsulated biomolecules.[3−5] Alternatively, self-assembling biomaterials that rely on physical cross-linking may yield or flow in response to variation in external shear stress (i.e., extrusion or spreading) during placement.[3,6] Upon removal of shear (i.e., after placement), such materials could potentially recover *in situ*,

thus providing local structure and delivery of biological cues in nonload bearing tissue sites.

Colloids are a promising candidate for this application. The cohesive strength of these materials is dependent on electrostatic forces, van der Waals attraction, and steric hindrance. These forces in combination directly influence the macroscopic material properties.[3−6] Of particular interest is the colloidal sol−gel transition, which is distinguished by a shift from dispersed solid particles at low concentrations to the formation of sample-spanning networks of particle flocculations at higher solid concentrations.[7−9] On the macroscopic level, this transition is marked by an appreciable increase in the material yield stress and viscosity.[7−9] Previous investigations have explored leveraging these interactions in oppositely charged poly(lactic-*co*-glycolic) acid nanoparticles,[4,5] gelatin nanoparticles,[10] and dextran microparticles[11,12] to form cohesive colloidal gels capable of delivering a variety of therapeutic osteogenic proteins for bone tissue engineering. More recently, nanoparticle gelatin colloidal gels were shown to outperform microparticle gelatin gels with regard to malleability during injection and as drug delivery vehicles *in vitro* and *in vivo*.[13,14] The current study aims to expand upon previous work

leveraging nanoparticle colloidal interactions by using biomolecules found in native human bone including hydroxyapatite (HAP) and glycosaminoglycans (GAGs).

HAP $[Ca_{10}(PO_4)_6(OH)_2]$ is a well-studied calcium orthophosphate bone substitute material similar to the mineral component of mammalian bones and is commonly referred to as "biological apatite".[15,16] HAP has been studied extensively in bone regeneration, and results indicate HAP nanoparticles (e.g., Ostim and Nanostim) can be delivered as highly concentrated colloidal pastes in injectable bone filler applications.[7,8,15−21] Phase separation has been observed in some HAP nanoparticle suspensions, leading to poor injectability or "filter-pressing"[17,22] and poor retention at the defect site,[23] resulting in limited tissue regeneration. Such limitations could be improved by incorporating large biomolecular polymers into the suspending fluid phase.[6,21,24−31] Polymer solutions exhibit a significant increase in viscosity with concentration due to increased entanglements or associations between polymer chains in the solution.[32−35] Additionally, polyelectrolytes (i.e., charged polymers) may be leveraged in a charged colloidal system to improve particle−polymer interactions to induce cohesiveness in the colloidal gel.[36]

Naturally occurring polymeric GAGs such as hyaluronic acid (HA) and chondroitin sulfate (CS) are found in extracellular matrix, cartilage, and skin. These GAGs exhibit desirable physicochemical properties as scaffolds in tissue engineering.[27,33−35,37,38] HA is a linear, high-molar-mass polysaccharide composed of alternating $(1 \rightarrow 4)$-β-linked D-glucuronic acid and $(1 \rightarrow 3)$-β-linked N-acetyl-D-glucosamine residues. CS differs only in the N-acetyl-D-glucosamine residue, which is sulfonated at either the 4 or 6 carbon site.[34,35,38,39] Because of repeating carboxyl or sulfonate moieties along the backbone, HA and CS occur as anionic macromolecules in aqueous environments at extracellular pH.[34,35,38,39] As a result, these highly charged macromolecules possess desirable shear-thinning and viscoelastic properties[32−34,37,38] and have primarily been used as inert carrier fluids in bone tissue engineering applications.[40] Emerging efforts, however, aim to elicit "bridging" connections within colloidal gels by using particles to act as anchoring points between multivalent, adsorbing polymers.[6,21,24−26,28−30,36,41,42]

In this study, polyanionic GAG polymers were combined with HAP nanoparticles in various concentrations and weight ratios to create cohesive "bridging" colloidal gels as potential scaffolds for bone tissue regeneration in irregular bone defects. This study represents the first attempt to exclusively combine native tissue components in a particle−polymer colloidal gel mixture with the goal of creating H−B fluids. More specifically, this study aims to elucidate the relationship between bulk rheological properties as a function of relative HAP nanoparticle and GAG biopolymer content. The primary goal of this assessment is to identify GAG−HAP colloidal gel candidates with appropriate yield stress, consistency, flow behavior, and recovery properties to explore surgical delivery in non-load-bearing bone regeneration applications.

2. EXPERIMENTAL SECTION

2.1. Materials. Hydroxyapatite was purchased as a powder ($D_{avg} \leq$ 200 nm (BET Analysis); Sigma-Aldrich). Chondroitin sulfate A from bovine trachea (M_w = 15−30 kDa) (Sigma-Aldrich, St. Louis, MO) and hyaluronic acid (M_w = 20−41 kDa) (Lifecore Biomedical, Chaska, MN) were purchased as sodium salts.

2.2. Characterization of HAP Nanoparticles. Size, morphology, and elemental distribution analysis of HAP were observed using a combination of transmission and scanning electron microscopy (TEM and SEM) and energy dispersive X-ray spectrometry (EDS) (FEI Tecnai F20 XT field emission TEM-EDS and Carl Zeiss Leo 1550 field emission scanning). Additional sizing and zeta-potential measurements of HAP were conducted using dynamic light scattering (Brookhaven, ZetaPALS).

Fourier transform infrared (FTIR) spectroscopy (PerkinElmer; Frontier FTIR) was used to confirm chemical identity. HAP samples were press formed into a thin disk with KBr crystals. The spectrum was collected in the 4000−400 cm^{-1} range with an average of 256 scans.

Crystallographic structural analysis of the sample was determined using the X-ray diffraction (XRD) method (Bruker; D8 Advance). Monochromatic Cu Kα radiation (λ = 0.154 06 nm) was used over the 2θ range of 20°−45° at a step size of 0.014° per 0.5 s. XRD data were compared with built-in Bruker software utilizing standard International Center for Diffraction Data (ICDD) for HAP.[15,16]

2.3. Preparation of Colloidal Gels. HA or CS powders were combined with HAP nanoparticles and dispersed in PBS solution (pH = 7.4, 150 mM NaCl). CS and HA concentrations in the mixtures were varied between 0 and 80% (w/v) and 0−40% (w/v), respectively. GAG:HAP weight ratio (w:w) was controlled by the incremental addition of HAP particles to GAG solutions at ratios of 2, 1, 0.5, 0.25, and 0.125. These mixtures were compared to pure component controls (GAG and HAP), respectively. Overall volume fraction of HAP ($\Phi = V_{HAP}/V_{mixture}$) was calculated from particle density and resulting mixture volume measurements. Homogeneous colloid mixtures were prepared by manual stirring (5 min) at ambient conditions and stored at 4 °C. Samples were allowed to equilibrate to ambient conditions (2 h) before testing.

2.4. Swelling Characterization. Relative swelling ratios (S) of CS−HAP and HA−HAP colloidal gels were determined by placing 1.0 mL of PBS (pH = 7.4, 150 mM NaCl) on top of 0.5 mL of material contained in a 2 mL Eppendorf tube. Tubes were then constantly agitated (24 h, 100 rpm, 37 °C) in an incubator shaker (New Brunswick Scientific, Excella E24). The swelling ratio ($S = (M_{(swollen)} - M_{(before)})/M_{(before)}$) was determined from the initial ($M_{(before)}$) and final ($M_{(swollen)}$) mass of the material as described by Holland et al.[43] The final weight was determined by removing excess PBS from tube and drying the surface of gel with evaporative paper.

2.5. Rheological Characterization. The rheological properties of the colloidal gels were characterized using a controlled stress rheometer (TA Instruments, AR2000). All measurements were performed using a stainless steel plate geometry (20 mm diameter) at a gap distance of 500 μm. The shear stress profile of the colloidal gels was determined using a stepped flow test (1 min/step) with an increasing shear rate (1−1000 s^{-1}). All samples were tested at 37 °C.

Recovery kinetics following temporary disruption of the colloidal gel network were determined by measuring viscoelastic properties as described by Ozbas et al.[44] Initially, an oscillatory stress sweep (1−1000 Pa) was performed at a constant frequency (1 Hz) to determine the linear viscoelastic (LVE) region. Subsequently, the gel viscoelastic properties including storage modulus (G′), loss modulus (G″), and loss angle (δ) were determined in a three-phase oscillatory time sweep at 37 °C following preshear (1 min, 100 s^{-1}) and equilibration (5 min). Gels were oscillated (5 min, low stress in LVE regime, 1 Hz) before and after an intense disruption phase (30 s, 1000 Pa, 1 Hz).

2.6. Rheological Modeling. Rheological flow property estimations were determined with a three-parameter fit to the H−B fluid model (eq 1)

$$\tau = \tau_y + K\dot{\gamma}^n \tag{1}$$

where τ was the measured shear stress [Pa] in the sample resulting from the fluid's yield stress, τ_y [Pa], consistency index, K [Pa·s^n], and flow behavior index, n [unitless], at a given shear rate, $\dot{\gamma}$ [s^{-1}]. The optimal fit was determined using the curve fitting tool software in MATLAB (The Mathworks, Inc.) with a nonlinear least-squares

method. Some GAG−HAP mixtures exhibited localized shear banding at low shear rates (<10 s^{-1}) as described by Møller et al.[45] As a result, data points below the critical shear rate, determined from the point of minimum shear stress in the sample, were excluded from H−B modeling. 95% confidence intervals were reported from triplicate measurements for all three parameters in each tested colloidal mixture along with the overall root-mean-squared error (RMSE) of the fit.

2.7. Statistical Analysis. All measurements were performed in triplicate ($n = 3$) and depicted as average ± standard deviation (SD) unless stated otherwise. Statistical analyses of data were performed using one-way analysis of variance (ANOVA), and Tukey's HSD was used post hoc to compare differences between individual groups. A p-value ($p < 0.05$) was accepted as statistically significant.

3. RESULTS

3.1. Characterization of HAP Nanoparticles. TEM-EDS analysis of HAP (Supporting Information Figure 1) revealed spherical particle morphology with polydisperse diameters near the supplier's specified value ($D_{avg} \leq 200$ nm (BET); Sigma-Aldrich); however, a small fraction of particles were visually observed to exceed this specification. SEM analysis of HAP, CS−HAP, and HA−HAP (Supporting Information Figures 2−4) likewise revealed spherical HAP particle morphology. Colloidal aggregation was also observed with SEM. However, negligible aggregation differences were observed between groups most likely due to the dehydrated state of the sample. Contrary to the supplier's elemental purity analysis ($\geq$97% HAP (wt %) (XRF Assay); Sigma-Aldrich), elemental distribution analysis (EDS) indicated the presence of calcium-deficient HAP (Supporting Information Figure 5). Atomic compositions of HAP samples were (average atomic % ± SD) Ca (24.58 ± 0.20%), P (15.91 ± 0.15%), and O (59.49 ± 0.30%), yielding a Ca/P ratio of 1.54. Pure stoichiometric HAP yields a Ca/P ratio of 1.67, while CDHA has a Ca/P ratio around $1.50-1.67$.[16] CDHA has been studied extensively in bone tissue regeneration due to its similar stoichiometry to that of "biological apatite".[17,46−48]

Dynamic light scattering was used to measure HAP particle size (nm) and zeta potential (mV) (average ± SD; $n = 10$). Dilute suspensions (0.167 mg/mL) of pure HAP particles where combined with either HA or CS in GAG:HAP weight ratios of 1:1 or 10:1, and the changes in size and zeta potential were observed (Table 1). Only the 10:1 ratio of CS:HAP

Table 1. HAP Dynamic Light Scattering Data[a]

weight ratio (GAG:HAP)	size (nm)	zeta potential (mV)
pure HAP	430 ± 73	−26.3 ± 5.5
CS:HAP (1:1)	520 ± 72	−49.5 ± 8.3**
CS:HAP (10:1)	540 ± 110*	−56.6 ± 6.2**
pure HAP	430 ± 73	−26.3 ± 5.5
HA:HAP (1:1)	490 ± 96	−39.4 ± 7.4**
HA:HAP (10:1)	470 ± 46	−45.8 ± 6.1**

[a]Significant differences between groups compared to pure HAP (ANOVA, post-hoc Tukey's HSD; $n = 15$; $p < 0.05$*; $p < 0.01$**).

resulted in a significant increase in particle size ($p < 0.05$) compared to the pure HAP. The inclusion of CS or HA at both weight ratios resulted in a significant increase in HAP zeta potential ($p < 0.01$) compared to the pure HAP suspensions.

FTIR spectra (Supporting Information Figure 6) of HAP revealed the presence of expected bonds in the crystal. Strong modes for stretching (1035 cm^{-1}) and bending (564, 604 cm^{-1}) indicated the presence of PO$_4$.[3−50] Characteristic

stretching (3572 cm^{-1}) of the −OH group was also observed.[49,50] Additionally, some bands indicating the weak presence of adsorbed water (1635 and 3000−3700 cm^{-1}) were observed.[49,50]

The XRD pattern (Supporting Information Figure 7) revealed expected HAP diffraction peaks at 2θ regions of 26°, 29°, 32°−34°, 40°, and 46°−54°, indicating the crystalline nature of the HAP particles when compared with the International Center for Diffraction Data (ICDD) for HAP.[49,50]

3.2. Swelling Characterization. Relative swelling of CS−HAP (Figure 1A) and HA−HAP (Figure 1B) gels increased with a clear dependence on HAP Φ. While sedimentation and swelling tolerances were initially set ($-20\% \leq S \leq 20\%$) in an attempt to identify suitable GAG−HAP candidates for retention of material at a bone defect surgical site, the most desirable colloidal mixtures exhibited the least amount of swelling or sedimentation ($S \approx 0\%$). Excessive sedimentation ($S \leq -20\%$) occurred in pure HAP mixtures below Φ = 0.25. The addition of CS or HA resulted in increased swelling at a given HAP Φ. Furthermore, swelling also exhibited dependence on GAG:HAP ratio (w:w), where mixtures with GAG in excess tended to show increased swelling and mixtures with HAP in excess tended to demonstrate swelling behavior of pure HAP. As a result, excessive sedimentation only occurred below HAP Φ = 0.12 and Φ = 0.06 for CS−HAP and HA−HAP colloidal mixtures, respectively. Excessive swelling ($S \geq +20\%$) occurred in mixtures containing GAG:HAP ratios in equivalence or in GAG excess ([1:1] and [2:1]) above Φ = 0.18. The only mixtures exhibiting excessive swelling and favoring HAP content were [1:2] GAG:HAP colloids with HAP concentrations above Φ = 0.37.

3.3. Rheological Characterization. *3.3.1. Consistency Index.* Measuring shear stress in response to increasing external shear rate yielded flow behavior properties which were estimated from a three-parameter H−B fluid model. An extensive array of CS−HAP (Supporting Information Table 1) and HA−HAP (Supporting Information Table 2) mixtures were tested and compared to pure HAP colloids (Supporting Information Table 3). Consistency index (K [Pa·s^n]) in CS−HAP and HA−HAP gels increased exponentially with increasing GAG content (% w/v) and increasing HAP content (% w/v) in the mixture, respectively. In addition, GAG−HAP mixtures containing HA had higher K values than respective CS mixtures. Plotting K values versus HAP Φ (Figure 2A,B) for constant GAG:HAP weight ratios (w:w) yielded a noticeable shift in K values from predominantly GAG-like behavior when in polymer excess to HAP-like behavior when in particle excess.

All tested mixtures, except those exhibiting high yield stress ($\tau_y > 500$ Pa), exhibited higher K values than the addition ($K_{GAG-HAP} \geq K_{GAG} + K_{HAP}$) of their respective pure GAG and HAP components. Examples of this synergistic K value behavior are seen in shear stress versus shear rate plots (Figure 3A,B), where the mixtures of 15% CS−60% HAP and 15% HA−60% HAP (% w/v) exhibited higher K values than predicted by the summation of their respective pure GAG 15% and pure HAP 60% components. Mixtures exhibiting high yield stress ($\tau_y \geq 500$ Pa) were the exception to this trend, where estimated K values were smaller than the addition of respective pure components. This likely reflects possible limitations attributed to how the H−B constitutive relationship captures τ_y and K behavior for some GAG−HAP mixtures. At high HAP concentrations, the increased apparent viscosity of the material
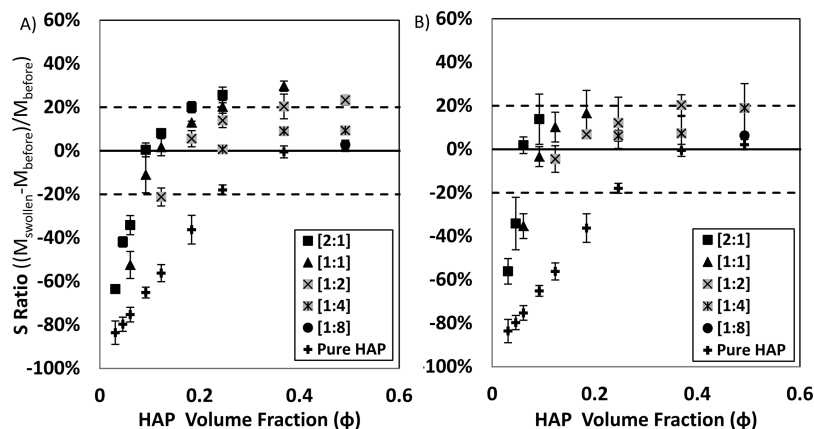
Figure 1. Swelling ratio of (A) CS−HAP and (B) HA−HAP gels plotted versus HAP Φ. Data sets represent GAG:HAP ratios (w:w) compared to pure HAP. No swelling change was desired ($S \approx 0$), and success criteria for the gels were established by setting swelling tolerances (dashed lines; $0 \pm 20\%$). Individual points are reported (average ± SD) from triplicate studies.

is modeled more by an increase in τ_y and not captured by K (Supporting Information Tables 1 and 2).

3.3.2. Flow Behavior Index. The flow behavior index (n [unitless]) of the pure aqueous PBS media was indicative of a Newtonian fluid ($n = 0.95 \pm 0.18$). In CS−HAP (Figure 2C) and HA−HAP (Figure 2D) mixtures, n values decreased from unity with the addition of HAP and GAG content, an indication of shear-thinning behavior ($n < 1$) in the gels. Further evidence of this was seen in plots containing n values versus HAP volume fraction (Φ) (Figure 2C,D) for constant GAG:HAP weight ratios (w:w). There was no conclusive evidence to support shear-thinning dependence on the concentration of GAG or GAG:HAP ratio in colloidal mixtures.

Examples elucidating the extent of shear thinning over the range of shear rates tested ($1−1000$ s^{-1}) was observed in log−log plots of viscosity versus shear rate for 15% CS−60% HAP and 15% HA−60% HAP (Figure 3C,D), respectively. While apparent viscosity was nearly independent of $\dot{\gamma}$ in pure GAG solutions such that n values were near unity ($n \approx 1$), GAG−HAP colloidal mixture viscosities decreased at least an order of magnitude over the tested shear rate range. These GAG−HAP mixtures exhibited high viscosities ($\mu > 100$ Pa·s) at lower shear rates and relatively low viscosities ($\mu < 10$ Pa·s) at higher shear rates.

3.3.3. Yield Stress. Yield stress (τ_y [Pa]) estimation from rheological data appeared to only be dependent on HAP particle concentration (Figure 2E,F), and an exponential increase in τ_y was seen across the entire range of tested HAP concentrations, 0%−80% (w/v) or $0.00 \leq \Phi \leq 0.49$. For some GAG−HAP mixtures H−B fluid modeling resulted in large confidence intervals and negative τ_y values (Supporting Information Tables 1 and 2). This likely reflects possible limitations attributed to how the H−B constitutive relationship captures τ_y and K behavior for some GAG−HAP mixtures, favoring an increase in τ_y instead of K at high HAP concentrations. Fluids with negative yield values were interpreted to possess no yield. Colloidal mixtures exhibited appreciable τ_y (≥ 10 Pa) only at the highest HAP concentrations 60−80% (w/v), which translated to a volume fraction of $\Phi = 0.37−0.49$. CS−HAP colloidal mixtures exhibited yield stress across all tested CS concentrations, while HA−HAP mixtures only exhibited τ_y below 20% HA (w/v).

3.3.4. Rheological and Swelling Summary. Tested CS−HAP (Figure 4A) and HA−HAP (Figure 4B) colloidal mixtures

were mapped on ternary diagrams (wt %). Based off of both swelling (S) and rheological properties (τ_y, K, and n) exhibited by each tested mixture, regions of desirable properties for facilitating surgical delivery were identified. Explicitly, a desirable mixture contained swelling or sedimentation within tolerance ($-20\% \leq S \leq +20\%$), identifiable yield stress ($\tau_y \geq 100$ Pa), and shear responsive flow properties ($n < 1$). From these criteria, 15% GAG−60% HAP mixtures were selected due to overlapping regions of desirable swelling and flow properties between CS and HA colloidal gels (Figure 4).

3.3.5. Viscoelastic Recovery. Selected colloidal gels were initially subjected to an oscillatory shear stress sweep ($1−1000$ Pa) at a constant frequency (1 Hz) to determine the linear viscoelastic (LVE) regime of the fluid. This was determined to be less than 100 Pa for all mixtures. Subsequent viscoelastic time sweeps were therefore conducted at an oscillatory shear stress selected to be sufficiently within the LVE regime for all samples ($10−25$ Pa). Viscoelastic properties including storage modulus (G'), loss modulus (G''), and phase angle (δ) of GAG−HAP mixtures were measured before, during, and after an intense temporary disruption period, which involved a large increase in external oscillatory shear stress on the material.

Based on previous swelling and flow behavior results, 15% GAG−60% HAP mixtures were selected as desirable candidates for viscoelastic recovery studies (Figure 5A,B) and then compared to their respective pure components at the same concentration. Recovery was assessed 5 min after disruption and expressed as a percentage ($G'_{recovery} = G'_{(Final)}/G'_{(Initial)} \times 100\%$) compared to initial G' in the mixture. Both the CS−HAP and HA−HAP mixtures recovered a large portion of their initial viscoelastic behavior within the brief recovery period, 64% and 85%, respectively. HA−HAP appeared to recover its initial G' within seconds of disruption while the CS−HAP mixture and pure HAP took several minutes. This may favor HA−HAP mixtures in a surgical application, since rapid self-assembly may improve retention in the tissue defect site. Pure HAP recovered a higher percentage, 92%, and pure CS and pure HA both recovered 100% of their initial viscoelastic properties almost instantaneously following disruption. Furthermore, G', G'', and δ values measured from GAG−HAP mixtures appeared to exhibit intermediate values between pure GAG and pure HAP components. Pure GAG exhibited primarily viscous behavior, and pure HAP exhibited predominately elastic behavior during periods of low oscillatory stress.
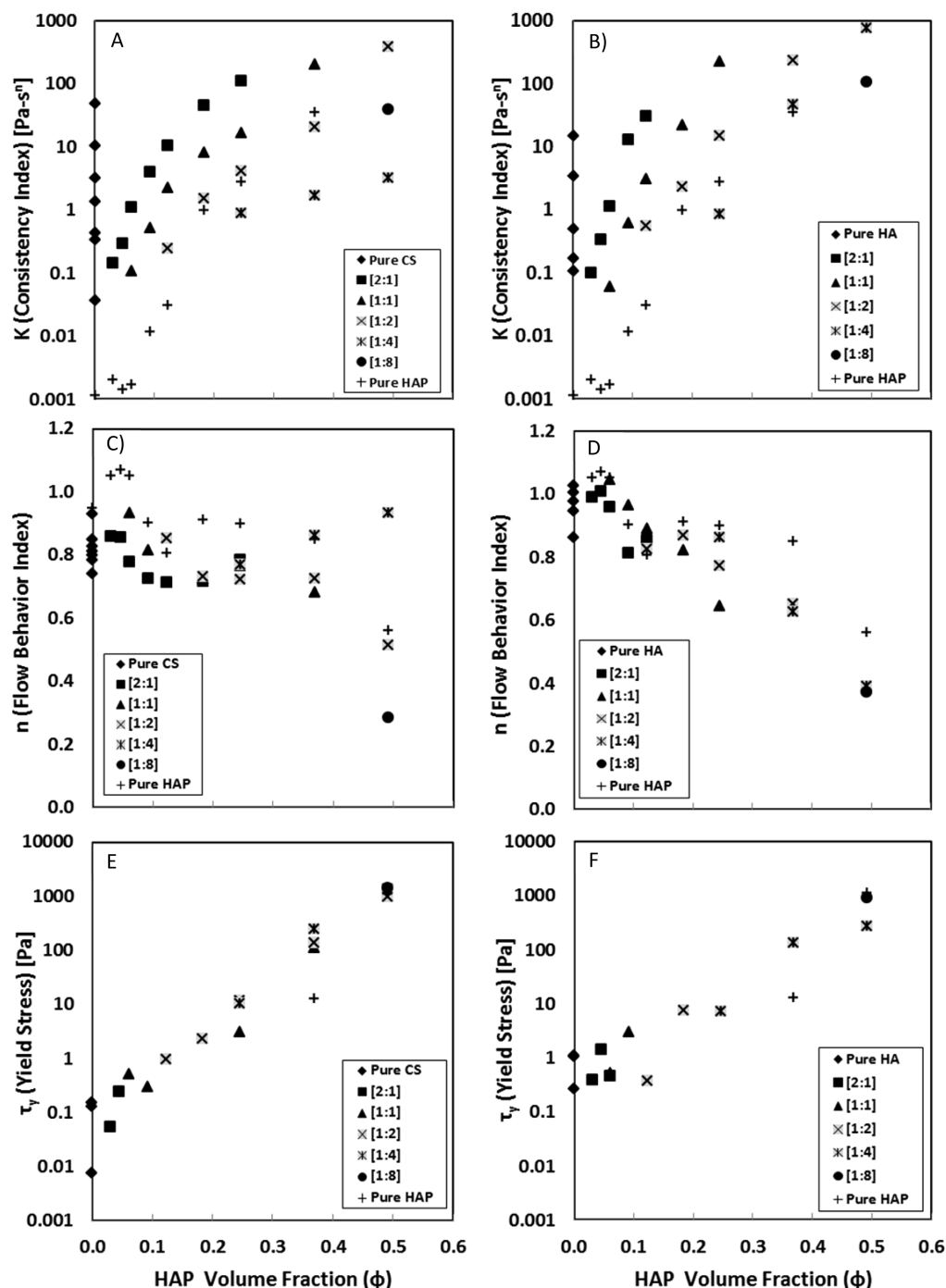
Figure 2. Trends in modeled H−B fluid parameters for K (A, B), n (C, D), and τ_y (E, F) plotted versus HAP Φ for CS−HAP (left) and HA−HAP (right) at various [GAG:HAP] ratios [w:w].

CS−HAP, HA−HAP, and pure HAP displayed primarily elastic behavior ($\delta \leq 14°$) during the initial low oscillatory stress phase, transitioned to predominately viscous behavior during the temporary disruption phase ($\delta \geq 84°$), and rapidly (<5 min) returned to primarily elastic behavior ($\delta \leq 16°$) while recovering from disruption at low oscillatory stress (Figure 5C,D). HA−HAP exhibited larger G' and G'' values than CS−HAP at the given GAG−HAP ratio.

4. DISCUSSION

Colloidal sols are suspensions of submicrometer particles undergoing Brownian motion.[3,6] Stabilization of these sols relies on the balance of particle−particle interactions such as electrostatic forces, van der Waals attraction, and steric hindrance.[3−6] Stable HAP sols have been created with the use of adsorbed polyelectrolytes that act as dispersing agents by forming steric barriers around particles.[51] However, these stable HAP sols generally possess a small consistency index and lack yield stress, which limit their application as bone tissue fillers.

Destabilized colloidal sols exhibit widespread flocculation across the colloidal mixture. When concentrations of particles are high enough, sample-spanning networks of flocculated particles are formed creating a colloidal gel.[7,52] In this study, pure HAP particles with spherical morphology and submi-
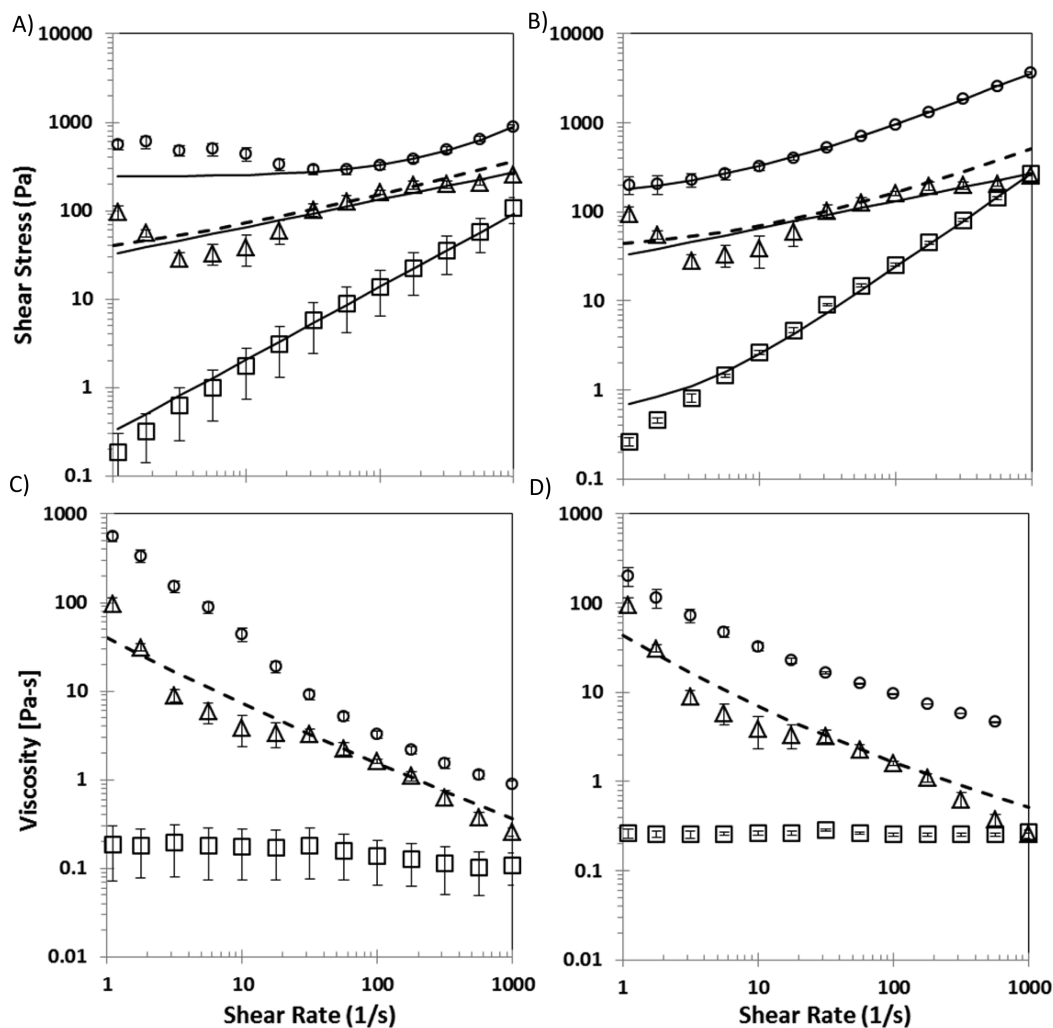
Figure 3. Examples of shear stress and viscosity profiles of CS 15%–HAP 60% (A, C) and HA 15%–HAP 60% (B, D) colloidal gels (circles) compared to pure components GAG 15% (squares) and HAP 60% (triangles). Displayed solid trend lines were calculated using a three-parameter fit to the H−B fluid model, and individual data points represent experimental average ± SD from triplicate studies. Dashed lines represent the H−B fit of experimental data from the addition of pure components GAG 15% and HAP 60%.

crometer diameter suspended in PBS media formed destabilized flocculations above 40% w/v as evidenced by significant sedimentation ($S \leq -20\%$) over 24 h (Figure 1A,B). Inclusion of polyelectrolytes can also induce substantial destabilization in colloids, where nonadsorbing polymers can induce depletion flocculation[53−55] and adsorbing polymers can induce flocculation by bridging.[53,56,57] In the latter case, particles act as cross-linkers between polymer molecules or vice versa. CS and HA contain repeat carboxylic acid moieties similar to poly(acrylic acid) and were hypothesized in this study to adsorb to the surface of the HAP particles via a similar mechanism.[51,52] The inclusion of either CS or HA at dilute HAP concentrations significantly increased overall zeta potential of HAP particles (Table 1), supporting the hypothesis that CS and HA adsorb to the particle surface. Although GAGs act to increase electrostatic stability at dilute concentrations, it is hypothesized that at high concentrations, similar to those tested in rheological experiments, bridging flocculation occurs due to multivalent GAG polymers adsorbing simultaneously to multiple HAP particles in close proximity.

The formation of sample spanning networks was observed macroscopically in swelling studies with the addition of CS and HA to suspensions of HAP, and the onset of these networks

appeared at lower total HAP Φ compared to pure HAP suspensions (Figure 1A,B). Swelling of the GAG−HAP mixtures was dependent on absolute GAG and HAP concentrations as well as relative GAG:HAP ratio, where mixtures favoring GAG content exhibited higher swelling compared to mixtures with HAP in excess. High concentrations of CS and HA exhibited undesirable swelling ($S \geq 20\%$), which may have been due to sodium salt associated with GAGs causing an osmotic pressure difference between the mixture and swelling media. The most desirable colloidal mixtures exhibited the least amount of swelling or sedimentation ($S \approx 0\%$) and were identified as suitable GAG−HAP candidates for enhancing retention of material at a tissue defect surgical site (Figure 4). This occurred only in mixtures containing both high concentrations of HAP ($\Phi \geq 0.36$) and GAG:HAP ratios favoring HAP ([1:4] and [1:8]).

More importantly, this study aimed to associate colloidal microstructure dynamics with observed synergistic rheological properties including τ_y, K, n, and $G'_{recovery}$. Critical boundaries of GAG−HAP colloidal mixtures were mapped with regard to potential tissue defect filling (Figure 4). The presence of τ_y was desired to improve chances of retention at a bone defect wound site, and therefore, a lack of τ_y (e.g., a liquid or phase-separated
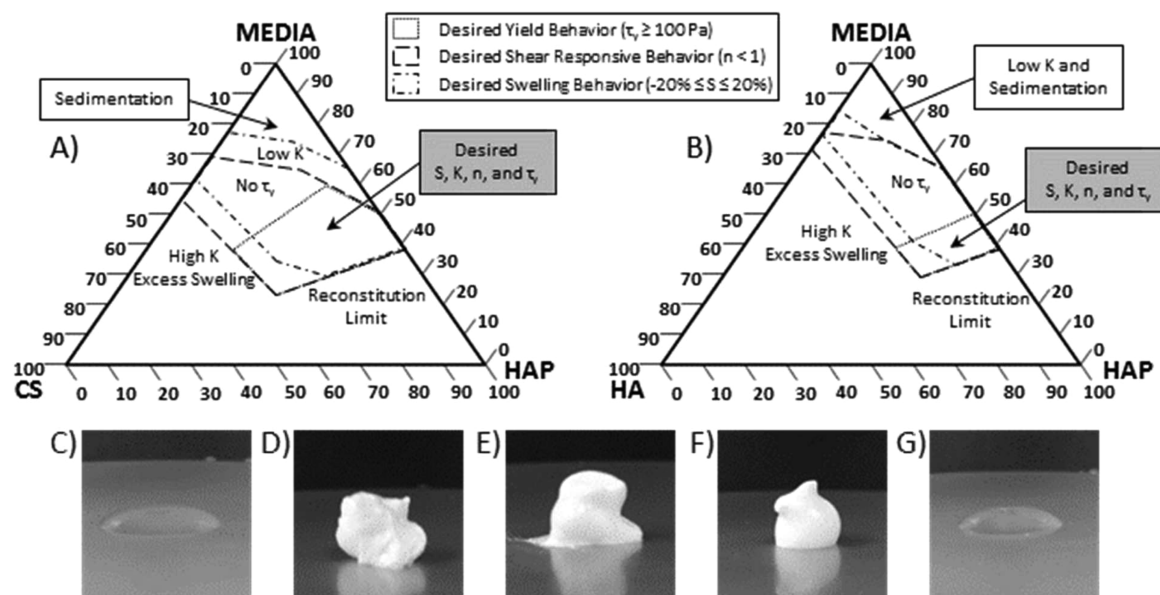
Figure 4. Ternary diagrams (wt %) for (A) CS−HAP and (B) HA−HAP colloidal mixtures identifying overlay of desirable regions of rheological yield (dotted line), shear-response (dashed line), and swelling properties (dot-dashed line). Images of extruded mixtures (via 21-gauge needle) of (C) pure CS (15%), (D) CS−HAP (15−60%), (E) pure HAP (60%), (F) HA−HAP (15−60%), and (G) pure HA (15%) (w/v).

suspension) was considered the minimum fail point in colloidal mixtures. Although a maximum τ_y limit was not defined, it was observed that mixtures containing more than 80% (w/v) HAP particles failed to reconstitute completely in PBS media. Therefore, this practical limit served as the basis for defining a maximum obtainable τ_y. The yield appeared to only be dependent on HAP (Figure 2E,F) within the tested concentration range, $0 \leq \Phi \leq 0.49$ (v/v). Furthermore, τ_y increased exponentially with increasing HAP Φ, where appreciable τ_y (>10 Pa) was observed only at the highest HAP concentrations 60−80% (w/v) or $\Phi = 0.37−0.49$, respectively. This observed transition corresponded with computer simulations and experiments on monodisperse colloidal hard spheres.[53,58] Below $\Phi < 0.49$ suspensions were reported to be disordered fluids exhibiting random local order; however, these networks can be sample-spanning and exhibit small amounts of τ_y.[53,58] Above $\Phi > 0.49$, suspensions became a mixture of colloidal fluid and colloidal crystals, where particles began ordering in macrocrystalline structure of either face-centered cubic or hexagonally close-packed orientation.[53,58] CS−HAP colloidal mixtures exhibited appreciable τ_y across all tested CS concentrations, but HA−HAP mixtures above 20% HA (w/v) possessed no yield regardless of HAP concentration. Since τ_y in these GAG−HAP mixtures was solely the result of HAP particle flocculation, the observed τ_y differences between CS and HA colloidal gels may have been caused by differences in the ability of the two GAGs to sterically hinder particle flocculation.

In addition to τ_y, GAG−HAP colloidal mixtures also exhibited significant viscosity changes over the range of shear rates tested (1−1000 s^{-1}) and were described by K and n in H−B fluid models. K and n behavior in high solid content HAP particle gels has been described previously[7,9,51,52] and were in agreement with tested pure HAP colloids. As particle concentrations become large enough to form sample-spanning flocculation networks, K undergoes a rapid increase due to the significant increase in attractive particle interactions.[7,9,51,52] Likewise, the K and n behaviors of pure HA solutions at various

molecular weights and concentrations have been observed[32,33,37] and appeared to be in agreement with pure HA solutions tested here. As polymer concentrations became larger, K values in the solution increased exponentially (Figure 2A,B). Previous work has attributed this exponential increase in polymer consistency to increased amounts of intermolecular entanglements.[32,33,37]

GAG−HAP mixtures tested here exhibited a synergistic increase in K compared to respective pure GAG and pure HAP components (Figure 2A,B), and this increase was seen clearly in the shear stress versus shear rate profiles for GAG 15%−HAP 60% colloidal gels (Figure 3A,B). The nature of this observed synergistic increase was most likely due to the GAG polymer chains inducing bridging flocculation between HAP particles.[3,6,26,28,53,56,57,59] Furthermore, the differences in K values exhibited by CS−HAP and HA−HAP gels were most likely a result of inherent K value differences in the respective GAG polymers combined with the nature of the particle flocculation induced by the addition of GAG polymer.[3,6,26,28,53,59]

Meanwhile, shear-thinning ($n < 1$) in colloidal gels occurs when the applied shear rate is high enough to disrupt the particle−particle spacing away from equilibrium.[53] Pure HAP and pure GAG mixtures exhibited shear-thinning behavior within the tested shear rate range (1−1000 s^{-s}) which was concentration dependent (Figure 2C,D). The addition of HAP into GAG-HAP mixtures enhanced shear-thinning behavior compared to pure GAG mixtures. Previous work with polymer−particle composites has also shown enhanced shear-thinning in these materials because shear rates experienced locally by a polymer confined between particles can be much larger than the overall external shear rate.[53]

Specific tolerance values for K and n were not predefined with regards to surgical application; however, these properties were shown to be highly tunable with respect to GAG and HAP concentrations. In general, higher consistency values were considered favorable since they coincided with enhanced shear responsive behavior including enhanced shear-thinning ($n < 1$) and viscoelastic recovery. Flow behavior results indicated a
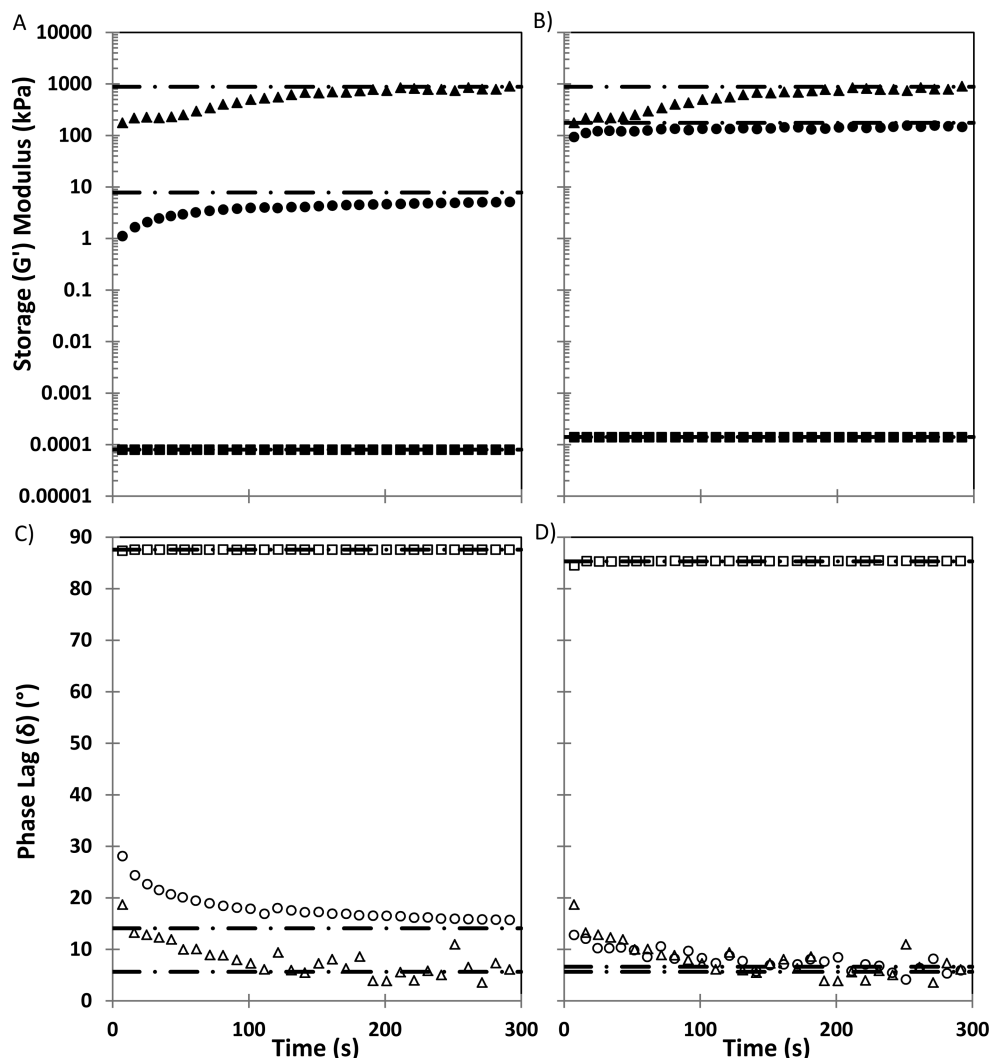
Figure 5. Viscoelastic recovery profiles of CS 15%−HAP 60% (A, C) and HA 15%−HAP 60% (B, D) gels (circles) were compared to pure components, GAG 15% (squares) and HAP (triangles) 60%. G' (solid symbols), G'' (not shown), and δ (open symbols) were measured every 3 s (n = 5) following a high oscillatory disruption phase. Recovery was assessed relative to a baseline low oscillatory stress profile for each group (dashed lines).

mutually beneficial relationship between K and n, where K values increased exponentially while shear-thinning behavior was enhanced with respective increase in GAG or HAP concentration. Additionally, it was shown that K was highly dependent on the polymer−particle ratio (w:w) in the GAG−HAP mixtures (Figure 2A,B). At high ratios where GAG was in excess, mixture properties were dominated by the polymer component. Likewise, at low ratios where HAP was in excess, mixture properties reflected those of pure HAP particles. Overall, flow experiments revealed that GAG−HAP colloidal mixtures could be tuned to exhibit large and synergistic K values without compromising shear-thinning behavior, a result that proves promising for surgical delivery purposes.

While the aforementioned rheological flow properties defined colloidal mixture behavior during shear-induced disruption (TOC figure; phase 1 → 2), oscillatory shear experiments attempted to elucidate GAG−HAP rheological recovery behavior following disruptive shear conditions. In these experiments, the colloidal mixture was allowed to recover initial viscoelastic properties following temporary microstructure breakdown (TOC figure; phase 2 → phase 3). A

malleable material desirable for non-load-bearing surgical application would possess a G' and G'' conducive to retention when no external force was present (e.g., primarily elastic behavior; $\delta < 45°$) and flow when exposed to an external shear (e.g., primarily viscous behavior; $\delta > 45°$). Additionally, a material with rapid recovery kinetics on the order of seconds to minutes following disruption (e.g., injection) may be desired. Utilizing results from swelling and rheological flow studies, colloidal mixtures containing 15% GAG−60% HAP exhibited the most desirable behavior among tested mixtures. Thus, dynamic viscoelastic recoveries of 15% GAG−60% HAP colloidal gels were compared to their pure GAG and HAP components, respectively (Figure 5A,B). In terms of G'_{recovery} magnitude, 15% GAG−60% HAP mixtures recovered less extensively compared to pure 60% HAP. This result was expected since return to particle spacing equilibrium following microstructure disruption is dependent on the particle diffusivity in the suspending fluid.[53,60] However, HA−HAP appeared to recover its initial G' within seconds of disruption while the CS−HAP mixture and pure HAP took several minutes. This may be due to the rapid and extensive self-

association of HA polymers in the mixture compared to CS.[32−34] This may favor HA−HAP mixtures in a tissue filler application, since rapid self-assembly may improve retention in the defect site. Overall, the rapid (<5 min) and extensive ($G'_{recovery} \geq 64\%$) recovery of viscoelastic properties in 15% GAG−60% HAP colloidal mixtures was encouraging with regard to potential surgical applications.

5. CONCLUSION

Malleable polymer−colloidal gels represent a desirable approach for minimally invasive filling of tissue defects and may ultimately facilitate regeneration of non-load-bearing bone defects. This study demonstrated that the addition of moderate molecular weight GAGs such as CS (M_w = 15−30 kDa) and HA (M_w = 20−41 kDa) can be used successfully to modify the rheological properties of submicrometer HAP ($D_{avg} \leq 200$ nm) colloidal gels. GAG−HAP colloidal mixtures appeared to exhibit substantial polymer−particle interactions, leading to a synergistic increase in consistency index (K) without compromising shear-thinning behavior ($n < 1$) of the gel. In addition, GAG−HAP colloids containing high concentrations of HAP exhibited substantial yield stress (τ_y) and viscoelastic recovery properties ($G'_{recovery}$) which may be desirable for retention of these materials at surgical sites. While rheological differences were observed between CS−HAP and HA−HAP colloidal gels, both CS and HA represent feasible options for future studies investigating bone defect filling. HA is available across a large range or molecular weights (10−1000s kDa) compared to CS, which may ultimately yield additional rheological advantages. Overall, this study mapped and identified desirable mixture regions (Figure 4A,B) where rheological properties of certain CS−HAP and HA−HAP colloidal gels aligned with desired properties to facilitate surgical delivery of fillers in non-load-bearing bone regeneration applications.

■ ASSOCIATED CONTENT

ⓈSupporting Information

Information on the TEM-EDS of HAP; SEM of HAP, CS−HAP, and HA−HAP; FT-IR of HAP; XRD patterns of HAP; H−B fluid table of values CS−HAP, HA−HAP, and pure HAP; viscoelastic recovery table. This material is available free of charge via the Internet at http://pubs.acs.org.

■ AUTHOR INFORMATION

Corresponding Author
*E-mail: berkland@ku.edu (C.J.B.).

Notes
The authors declare no competing financial interest.

■ ACKNOWLEDGMENTS

■ ABBREVIATIONS

CS, chondroitin sulfate; GAG, glycosaminoglycan; HA, hyaluronic acid; HAP, hydroxyapatite; H−B, Herschel−Bulkley fluid; LVE, linear viscoelastic region.

■ REFERENCES

(1) Roux, R.; Ladaviere, C.; Montembault, A.; Delair, T. Particle assemblies: Toward new tools for regenerative medicine. *Mater. Sci. Eng., C* **2013**, 33 (3), 997−1007.

(2) Temenoff, J. S.; Mikos, A. G. Injectable biodegradable materials for orthopedic tissue engineering. *Biomaterials* **2000**, 21 (23), 2405−12.

(3) Guvendiren, M.; Lu, H. D.; Burdick, J. A. Shear-thinning hydrogels for biomedical applications. *Soft Matter* **2012**, 8 (2), 260−272.

(4) Wang, Q.; Jamal, S.; Detamore, M. S.; Berkland, C. PLGA-chitosan/PLGA-alginate nanoparticle blends as biodegradable colloidal gels for seeding human umbilical cord mesenchymal stem cells. *J. Biomed. Mater. Res., Part A* **2011**, 96 (3), 520−7.

(5) Wang, Q.; Wang, J.; Lu, Q.; Detamore, M. S.; Berkland, C. Injectable PLGA based colloidal gels for zero-order dexamethasone release in cranial defects. *Biomaterials* **2010**, 31 (18), 4980−6.

(6) Lin, Y.; Boker, A.; He, J.; Sill, K.; Xiang, H.; Abetz, C.; Li, X.; Wang, J.; Emrick, T.; Long, S.; Wang, Q.; Balazs, A.; Russell, T. P. Self-directed self-assembly of nanoparticle/copolymer mixtures. *Nature* **2005**, 434 (7029), 55−9.

(7) Cunningham, E.; Dunne, N.; Walker, G.; Buchanan, F. High-solid-content hydroxyapatite slurry for the production of bone substitute scaffolds. *Proc. Inst. Mech. Eng., Part H* **2009**, 223 (6), 727−37.

(8) Huber, F. X.; McArthur, N.; Heimann, L.; Dingeldein, E.; Cavey, H.; Palazzi, X.; Clermont, G.; Boutrand, J. P. Evaluation of a novel nanocrystalline hydroxyapatite paste Ostim in comparison to Alpha-BSM - more bone ingrowth inside the implanted material with Ostim compared to Alpha BSM. *BMC Musculoskeletal Disord.* **2009**, 10, 164.

(9) Kilfoil, M. L.; Pashkovski, E. E.; Masters, J. A.; Weitz, D. A. Dynamics of weakly aggregated colloidal particles. *Philos. Trans. R. Soc., A* **2003**, 361 (1805), 753−64 discussion 764−6.

(10) Wang, H.; Hansen, M. B.; Lowik, D. W.; van Hest, J. C.; Li, Y.; Jansen, J. A.; Leeuwenburgh, S. C. Oppositely charged gelatin nanospheres as building blocks for injectable and biodegradable gels. *Adv. Mater.* **2011**, 23 (12), H119−24.

(11) Van Tomme, S. R.; van Nostrum, C. F.; de Smedt, S. C.; Hennink, W. E. Degradation behavior of dextran hydrogels composed of positively and negatively charged microspheres. *Biomaterials* **2006**, 27 (22), 4141−8.

(12) Van Tomme, S. R.; van Steenbergen, M. J.; De Smedt, S. C.; van Nostrum, C. F.; Hennink, W. E. Self-gelling hydrogels based on oppositely charged dextran microspheres. *Biomaterials* **2005**, 26 (14), 2129−35.

(13) Wang, H.; Boerman, O. C.; Sariibrahimoglu, K.; Li, Y.; Jansen, J. A.; Leeuwenburgh, S. C. Comparison of micro- vs. nanostructured colloidal gelatin gels for sustained delivery of osteogenic proteins: Bone morphogenetic protein-2 and alkaline phosphatase. *Biomaterials* **2012**, 33 (33), 8695−703.

(14) Wang, H.; Zou, Q.; Boerman, O. C.; Nijhuis, A. W.; Jansen, J. A.; Li, Y.; Leeuwenburgh, S. C. Combined delivery of BMP-2 and bFGF from nanostructured colloidal gelatin gels and its effect on bone regeneration in vivo. *J. Controlled Release* **2013**, 166 (2), 172−81.

(15) Detsch, R.; Hagmeyer, D.; Neumann, M.; Schaefer, S.; Vortkamp, A.; Wuelling, M.; Ziegler, G.; Epple, M. The resorption of nanocrystalline calcium phosphates by osteoclast-like cells. *Acta Biomater.* **2010**, 6 (8), 3223−33.

(16) Dorozhkin, S. V. Nanosized and nanocrystalline calcium orthophosphates. *Acta Biomater.* **2010**, 6 (3), 715−34.

(17) Bohner, M. Design of ceramic-based cements and putties for bone graft substitution. *Eur. Cells Mater.* **2010**, 20, 1−12.

(18) Huber, F. X.; Hillmeier, J.; Kock, H. J.; McArthur, N.; Huber, C.; Diwo, M.; Baier, M.; Meeder, P. J. Filling of metaphyseal defects with nanocrystalline hydroxyapatite (Ostim) for fractures of the radius. *Zentralbl. Chir.* **2008**, 133 (6), 577−81.

(19) Tadic, D.; Epple, M. A thorough physicochemical character-isation of 14 calcium phosphate-based bone substitution materials in comparison to natural bone. *Biomaterials* **2004**, 25 (6), 987−94.

(20) Thorwarth, M.; Schultze-Mosgau, S.; Kessler, P.; Wiltfang, J.; Schlegel, K. A. Bone regeneration in osseous defects using a resorbable nanoparticular hydroxyapatite. *J. Oral Maxillofac. Surg.* **2005**, *63* (11), 1626–33.

(21) Zhao, L.; Weir, M. D.; Xu, H. H. An injectable calcium phosphate-alginate hydrogel-umbilical cord mesenchymal stem cell paste for bone tissue engineering. *Biomaterials* **2010**, *31* (25), 6502–10.

(22) Habib, M.; Baroud, G.; Gitzhofer, F.; Bohner, M. Mechanisms underlying the limited injectability of hydraulic calcium phosphate paste. Part II: particle separation study. *Acta Biomater.* **2010**, *6* (1), 250–6.

(23) Verma, N. P.; Sinha, A. Effect of solid to liquid ratio on the physical properties of injectable nanohydroxyapatite. *J. Mater. Sci.: Mater. Med.* **2013**, *24* (1), 53–9.

(24) Balazs, A. C.; Emrick, T.; Russell, T. P. Nanoparticle polymer composites: where two small worlds meet. *Science* **2006**, *314* (5802), 1107–10.

(25) Huang, Z.; Tian, J.; Yu, B.; Xu, Y.; Feng, Q. A bone-like nano-hydroxyapatite/collagen loaded injectable scaffold. *Biomed. Mater.* **2009**, *4* (5), 055005.

(26) Laurati, M.; Petekidis, G.; Koumakis, N.; Cardinaux, F.; Schofield, A. B.; Brader, J. M.; Fuchs, M.; Egelhaaf, S. U. Structure, dynamics, and rheology of colloid-polymer mixtures: from liquids to gels. *J. Chem. Phys.* **2009**, *130* (13), 134907.

(27) Sundaram, H.; Voigts, B.; Beer, K.; Meland, M. Comparison of the rheological properties of viscosity and elasticity in two categories of soft tissue fillers: calcium hydroxylapatite and hyaluronic acid. *Dermatol. Surg.* **2010**, *36* (Suppl. 3), 1859–65.

(28) Surve, M.; Pryamitsyn, V.; Ganesan, V. Polymer-bridged gels of nanoparticles in solutions of adsorbing polymers. *J. Chem. Phys.* **2006**, *125* (6), 64903.

(29) Surve, M.; Pryamitsyn, V.; Ganesan, V. Universality in structure and elasticity of polymer-nanoparticle gels. *Phys. Rev. Lett.* **2006**, *96* (17), 177805.

(30) Surve, M.; Pryamitsyn, V.; Ganesan, V. Nanoparticles in solutions of adsorbing polymers: pair interactions, percolation, and phase behavior. *Langmuir* **2006**, *22* (3), 969–81.

(31) Tian, X. Y.; Li, M. G.; Cao, N.; Li, J. W.; Chen, X. B. Characterization of the flow behavior of alginate/hydroxyapatite mixtures for tissue scaffold fabrication. *Biofabrication* **2009**, *1* (4), 045005.

(32) Berriaud, N.; Milas, M.; Rinaudo, M. Rheological study on mixtures of different molecular weight hyaluronates. *Int. J. Biol. Macromol.* **1994**, *16* (3), 137–42.

(33) Matteini, P.; Dei, L.; Carretti, E.; Volpi, N.; Goti, A.; Pini, R. Structural behavior of highly concentrated hyaluronan. *Biomacromolecules* **2009**, *10* (6), 1516–22.

(34) Seyrek, E.; Dubin, P. Glycosaminoglycans as polyelectrolytes. *Adv. Colloid Interface Sci.* **2010**, *158* (1–2), 119–29.

(35) Volpi, N.; Schiller, J.; Stern, R.; Soltes, L. Role, metabolism, chemical modifications and applications of hyaluronan. *Curr. Med. Chem.* **2009**, *16* (14), 1718–45.

(36) Roux, R.; Ladaviere, C.; Montembault, A.; David, L.; Delair, T. Shear thinning three-dimensional colloidal assemblies of chitosan and poly(lactic acid) nanoparticles. *J. Phys. Chem. B* **2013**, *117* (24), 7455–64.

(37) Stocks, D.; Sundaram, H.; Michaels, J.; Durrani, M. J.; Wortzman, M. S.; Nelson, D. B. Rheological evaluation of the physical properties of hyaluronic acid dermal fillers. *J. Drugs Dermatol.* **2011**, *10* (9), 974–80.

(38) Silbert, J. E.; Sugumaran, G. Biosynthesis of chondroitin/dermatan sulfate. *IUBMB Life* **2002**, *54* (4), 177–86.

(39) Buzzega, D.; Maccari, F.; Volpi, N. Determination of molecular mass values of chondroitin sulfates by fluorophore-assisted carbohydrate electrophoresis (FACE). *J. Pharm. Biomed. Anal.* **2010**, *51* (4), 969–72.

(40) Gruskin, E.; Doll, B. A.; Futrell, F. W.; Schmitz, J. P.; Hollinger, J. O. Demineralized bone matrix in bone repair: history and use. *Adv. Drug Delivery Rev.* **2012**, *64* (12), 1063–77.

(41) Lim, J. J.; Hammoudi, T. M.; Bratt-Leal, A. M.; Hamilton, S. K.; Kepple, K. L.; Bloodworth, N. C.; McDevitt, T. C.; Temenoff, J. S. Development of nano- and microscale chondroitin sulfate particles for controlled growth factor delivery. *Acta Biomater.* **2011**, *7* (3), 986–95.

(42) Lu, H. D.; Charati, M. B.; Kim, I. L.; Burdick, J. A. Injectable shear-thinning hydrogels engineered with a self-assembling Dock-and-Lock mechanism. *Biomaterials* **2012**, *33* (7), 2145–53.

(43) Holland, T. A.; Tabata, Y.; Mikos, A. G. In vitro release of transforming growth factor-beta 1 from gelatin microparticles encapsulated in biodegradable, injectable oligo(poly(ethylene glycol) fumarate) hydrogels. *J. Controlled Release* **2003**, *91* (3), 299–313.

(44) Ozbas, B.; Rajagopal, K.; Haines-Butterick, L.; Schneider, J. P.; Pochan, D. J. Reversible stiffening transition in beta-hairpin hydrogels induced by ion complexation. *J. Phys. Chem. B* **2007**, *111* (50), 13901–8.

(45) Møller, P. C. F.; Mewis, J.; Bonn, D. Yield stress and thixotropy: on the difficulty of measuring yield stresses in practice. *Soft Matter* **2006**, *2* (4), 274–283.

(46) LeGeros, R. Z. Properties of osteoconductive biomaterials: calcium phosphates. *Clin. Orthop. Relat. Res.* **2002**, *395*, 81–98.

(47) Supova, M. Problem of hydroxyapatite dispersion in polymer matrices: a review. *J. Mater. Sci.: Mater. Med.* **2009**, *20* (6), 1201–13.

(48) Swetha, M.; Sahithi, K.; Moorthi, A.; Srinivasan, N.; Ramasamy, K.; Selvamurugan, N. Biocomposites containing natural polymers and hydroxyapatite for bone tissue engineering. *Int. J. Biol. Macromol.* **2010**, *47* (1), 1–4.

(49) Bao, X.; P, Y. X. Influence of temperature, ripening time and calcination on the morphology and crystallinity of hydroxyapatite nanoparticles. *J. Eur. Ceram. Soc.* **2002**, *23*, 1697–1704.

(50) Murugan, R.; Ramakrishna, S. Bioresorbable composite bone paste using polysaccharide based nano hydroxyapatite. *Biomaterials* **2004**, *25* (17), 3829–35.

(51) Bao, Y.; Senos, A. M.; Almeida, M.; Gauckler, L. J. Rheological behavior of aqueous suspensions of hydroxyapatite (HAP). *J. Mater. Sci.: Mater. Med.* **2002**, *13* (7), 639–43.

(52) Gardini, D.; Galassi, C. Rheology of hydoxyapatite dispersions. *J. Am. Ceram. Soc.* **2005**, *88* (2), 271–276.

(53) Larson, R. G. *The Structure and Rheology of Complex Fluids*; Oxford University Press: New York, 1999.

(54) Asakura, S.; Oosawa, F. Interaction between particles suspended in solutions of macromolecules. *J. Polym. Sci.* **1958**, *33* (126), 183–192.

(55) Jenkins, P.; Snowden, M. Depletion flocculation in colloidal dispersions. *Adv. Colloid Interface Sci.* **1996**, *68*, 57–96.

(56) Otsubo, Y. Rheology control of suspensions by soluble polymers. *Langmuir* **1995**, *11* (6), 1893–1898.

(57) Wen, Y. H.; Lin, P. C.; Lee, C. Y.; Hua, C. C.; Lee, T. C. Reduced colloidal repulsion imparted by adsorbed polymer of particle dimensions. *J. Colloid Interface Sci.* **2010**, *349* (1), 134–41.

(58) Segre, P. N.; Meeker, S. P.; Pusey, P. N.; Poon, W. C. K. Viscosity and structural relaxation in suspensions of hard-sphere colloids. *Phys. Rev. Lett.* **1995**, *75* (5), 958–961.

(59) Roux, R.; Ladaviere, C.; Montembault, A.; Delair, T. Paricle assemblies: Toward new tools for regenerative medicine. *Mater. Sci. Eng., C* **2013**, *33*, 997–1007.

(60) Choi, G. N.; Krieger, I. M. Rheological studies on sterically stabilized dispersions of uniform colloidal spheres. *J. Colloid Interface Sci.* **1986**, *113* (1), 94–100.